

Electronic Supplementary Information

Novel natural myricetin with AIE and ESIPT characteristics for selective detection and imaging of superoxide anion *in vitro* and *in vivo*

Ruiqing Long,^a Cui Tang,^b Qiachi Fu,^a Jinju Xu,^a Te Li,^a Chaoying Tong,^a Ying Guo,^{b,*}
Lihui Wu,^a Shuyun Shi^{a,c,*} and Daijie Wang^c

^aKey Laboratory of Hunan Province for Water Environment and Agriculture Product Safety, College of Chemistry and Chemical Engineering, Central South University, Changsha 410083, China. E-mail: shuyshi@gmail.com

^bDepartment of Clinical Pharmacology, Xiangya Hospital; Hunan Key Laboratory of Pharmacogenetics, Central South University, 410078 Changsha, China. E-mail: guoying881212@csu.edu.cn

^cKey Laboratory of TCM Quality Control, Shandong Analysis and Test Center, Qilu University of Technology (Shandong Academy of Sciences), Jinan 250014, China

1. Experimental section

1.1. Materials

Lipopolysaccharide (LPS), phorbol-12-myristate-13-acetate (PMA), and 4,5-dihydroxy-1,3-benzenedisulfonic acid disodium salt (Tiron) were acquired from Macklin Reagent Co., Ltd. (Shanghai, China). Tetrahydrofuran (THF), methylthiazolyldiphenyl-tetrazolium bromide (MTT), dimethylsulfoxide (DMSO) and KO_2 were bought from Aladdin Reagent Co., Ltd. (Shanghai, China). FeCl_2 , NaClO , H_2O_2 , NaNO_2 , ethanol, petroleum ether, and ethyl acetate were purchased from China National Medicines Co., Ltd. (Beijing, China). Glutathione (GSH) was bought from Aladdin (Shanghai, China). Physiological saline was provided by local drug store (Changsha, China). Chloral hydrate was from Xiangya hospital, Central South University (Changsha, China). All the chemicals and reagents were of analytical grade without additional purification. Ultrapure water (18.2 M Ω) was purified and filtered using a Milli-Q water purification system (Millipore, Bedford, MA, USA).

1.2. Instruments

^1H -NMR and ^{13}C -NMR spectra were recorded on Bruker 400 spectrometer with chemical shifts reported in ppm and coupling constants (J) reported in Hz. High resolution mass spectra (HRMS) were obtained by Bruker compact QTOF-MS with an electrospray ionization (ESI) interface (Bruker Co., Bremen, Germany). FI-TR spectra were collected by the IR Prestige-21 Fourier transform infrared (FTIR) (Shimadzu, Japan). TEM images were obtained using Tecnai G2 20S-Twin transmission electron microscope (TEM, FEI, Prague, Czech). The PHI Quantera II X-ray photoelectron spectroscopy (XPS, Thermo Fisher Scientific Inc., Waltham, MA) was employed to investigate the surface functional properties of myricetin nanocrystals. The fluorescence measurements were carried out on a Perkin-Elmer LS-55 luminescence

spectrometer (PerkinElmer, USA). UV-vis spectra were recorded on the UV-2600 spectrophotometer (Shimadzu, Japan). Fluorescence lifetime was measured with Fluo Time 100 (PicoQuant, Germany). pH value was controlled using Five Easy plus pH Meter (Mettler Toledo, China). Cell imaging was studied by Snap cool HQ² imaging system (Photometrics Inc., USA). Animal experiments were carried out on IVIS lumina (PerkinElmer, USA).

1.3. Preparative isolation of myricetin from vine tea

Vine tea was collected in May 2017 from Jianghua, Hunan, China. The plant material was identified by Prof. Zhaoming Xie, Research Institute of Chinese Medicine, Hunan Academy of Chinese Medicine, Changsha, China. After collection, vine tea was immediately dried at 40 °C in an oven with air circulation. Dry vine tea was ground and sieved, and materials between 180 and 250 μm was used for extraction. Vine tea powder (50.0 g) was extracted with 70% ethanol (250 mL, three times) at 85 °C (each for 3 h). After filtration, the extract was combined and evaporated to dryness (22.6 g). Crude extract (11.0 g) was chromatographed on repeated silica gel columns using petroleum ether–ethyl acetate (1:0–0:1) as solvent systems to afford 120.3 mg of myricetin.

1.4. Computation Methods.

Time-dependent density functional theory (TD-DFT) calculations were used for the theoretical investigation of ESIPT mechanism. Local minima and transition state structures were obtained by optimization of geometry. Geometries were determined with the B3LYP/6-31+G (d) basis set, while energies were determined by single point calculations with the B3LYP/6-311+G (d,p) basis set upon optimized structures. All calculations were performed using GaussView 5.0 package.

1.5. Responses of myricetin nanocrystals to reactive oxygen species

Superoxide anion ($O_2^{\bullet-}$) was obtained using KO_2 dissolved in DMSO, and the

concentration of KO_2 was determined with UV-vis spectra. Hydroxyl radical ($\bullet\text{OH}$) was generated by mixing Fe^{2+} (30 mM) with H_2O_2 (3 mM), and the concentration of $\bullet\text{OH}$ was equal to the Fe^{2+} concentration. Single oxygen ($^1\text{O}_2$) was produced by addition H_2O_2 (30 mM) to NaClO (30 mM) under nitrogen atmosphere. Peroxynitrite (ONOO^-) was prepared using H_2O_2 (35 mM) and NaNO_2 (30 mM). Hypochlorite ion (ClO^-) was provided by NaClO , and the concentration of ClO^- was determined based on the molar extinction coefficient at 292 nm ($350 \text{ l (M}\cdot\text{cm)}^{-1}$).

Myricetin (100 μg) is dissolved in 10 mL THF/ H_2O (20/80) solution. Then the mixtures were sonicated for 2 h at 25 $^\circ\text{C}$ and placed in a fume hood to volatilize all the THF for preparation of myricetin nanocrystals. Different concentrations (0, 0.3, 5, 10, 15, 18, 20, 23, 30 mM) of reactive oxygen species solutions (3.0 μL) were mixed with myricetin nanocrystal solution (3.0 mL). Mixtures were placed at 25 $^\circ\text{C}$ for 30 s, and then fluorescence (FL) spectra were measured. The excitation wavelength, excitation and emission silts were set at 350, 5, and 20 nm, respectively.

Meanwhile, MS spectrum of the myricetin- $\text{O}_2^{\bullet-}$ mixtures was taken to evaluate the chemical reaction between myricetin and $\text{O}_2^{\bullet-}$.

1.6. Cytotoxicity and cellular imaging investigation

Cytotoxicity of myricetin nanocrystals was evaluated using MTT assay. HeLa cells were supported by Xiangya Hospital of Central South University. HeLa cells were seeded in 96-well plate with the density of 1×10^4 cells per each well and attached for 24 h in cell culture medium at 5 % CO_2 atmosphere. Then, HeLa cells were treated with myricetin nanocrystals with final concentrations of 0, 0.05, 0.1, 0.2, 0.3, 0.4, 0.6, 0.8 and 1.0 mg mL^{-1} , and incubated for another 24 h at 5 % CO_2 atmosphere. Freshly prepared MTT (150 μL , 0.5 mg mL^{-1}) was added to each well to form the violet formazan for 4 h. Supernatant was removed and DMSO (150 μL) was added and shaken

for 15 min to dissolve the violet formazan. Optical density (OD) of each well was measured using Enzyme Linked Immunosorbent Assay reader at 490 nm. Cell viability was calculated as following: cell viability (%) = $(OD_{\text{treated}}/OD_{\text{control}}) \times 100\%$, where OD_{treated} and OD_{control} were obtained with and without treatment with myricetin nanocrystals.

For cellular imaging, HeLa cells were seeded in 6-well plate with the density of 7×10^4 cells per each well and attached for 24 h in cell culture medium at 5 % CO₂ atmosphere. HeLa cells were treated with myricetin nanocrystals ($100 \mu\text{g mL}^{-1}$, 1.5 mL) at 37°C for 4 h. After that, the medium was removed and the cells were rinsed three times with PBS buffer (100 mM, pH 7.4). Then, cells were treated with LPS for 3 h ($5 \mu\text{g mL}^{-1}$, 1.5 mL) and PMA ($1 \mu\text{g mL}^{-1}$, 1.5 mL) for 0.5 h, respectively. After removal of the media and washed with PBS buffer (100 mM, pH 7.4) twice, HeLa cells were imaged by confocal laser scanning microscope.

For control experiments, HeLa cells were treated with LPS for 3 h ($5 \mu\text{g mL}^{-1}$, 1.5 mL) and PMA ($1 \mu\text{g mL}^{-1}$, 1.5 mL) for 0.5 h, respectively. After removal of the media and washed with PBS buffer (100 mM, pH 7.4) twice, HeLa cells were imaged by confocal laser scanning microscope.

1.7. LPS-induced inflammation in mice

All animal experiments were in accordance with the Principles of Laboratory Animal Care (People's Republic of China), and approved by the Animal Care and Use Committee of Xiangya Hospital, Central South University. Female ICR mice (eight-to-ten weeks old) were divided into four groups to be treated with different conditions. Saline group: mice were intraperitoneally injected with physiological saline (200 μL). LPS group: mice were intraperitoneally injected with LPS (1mg mL^{-1} in saline, 200 μL) to induce acute inflammation. LPS and Tiron group: Mice were intraperitoneally

injected with LPS (1mg mL^{-1} in saline, $200\ \mu\text{L}$). Tiron was then injected after three hours. Four hours later, mice were anesthetized by intraperitoneal injection of 4% chloral hydrate ($3\ \text{mL kg}^{-1}$), and the abdominal fur was removed. And then, myricetin nanocrystals ($100\ \mu\text{g}$ in saline) was injected to mice. For control group, mice were intraperitoneally injected with LPS (1mg mL^{-1} in saline, $200\ \mu\text{L}$) without myricetin nanocrystals. Images were obtained using IVIS lumina series III in vivo imaging system with open filter as soon as possible. The excitation and emission wavelengths were 440 and 620 nm.

2. Supplementary Fig. S1-S9

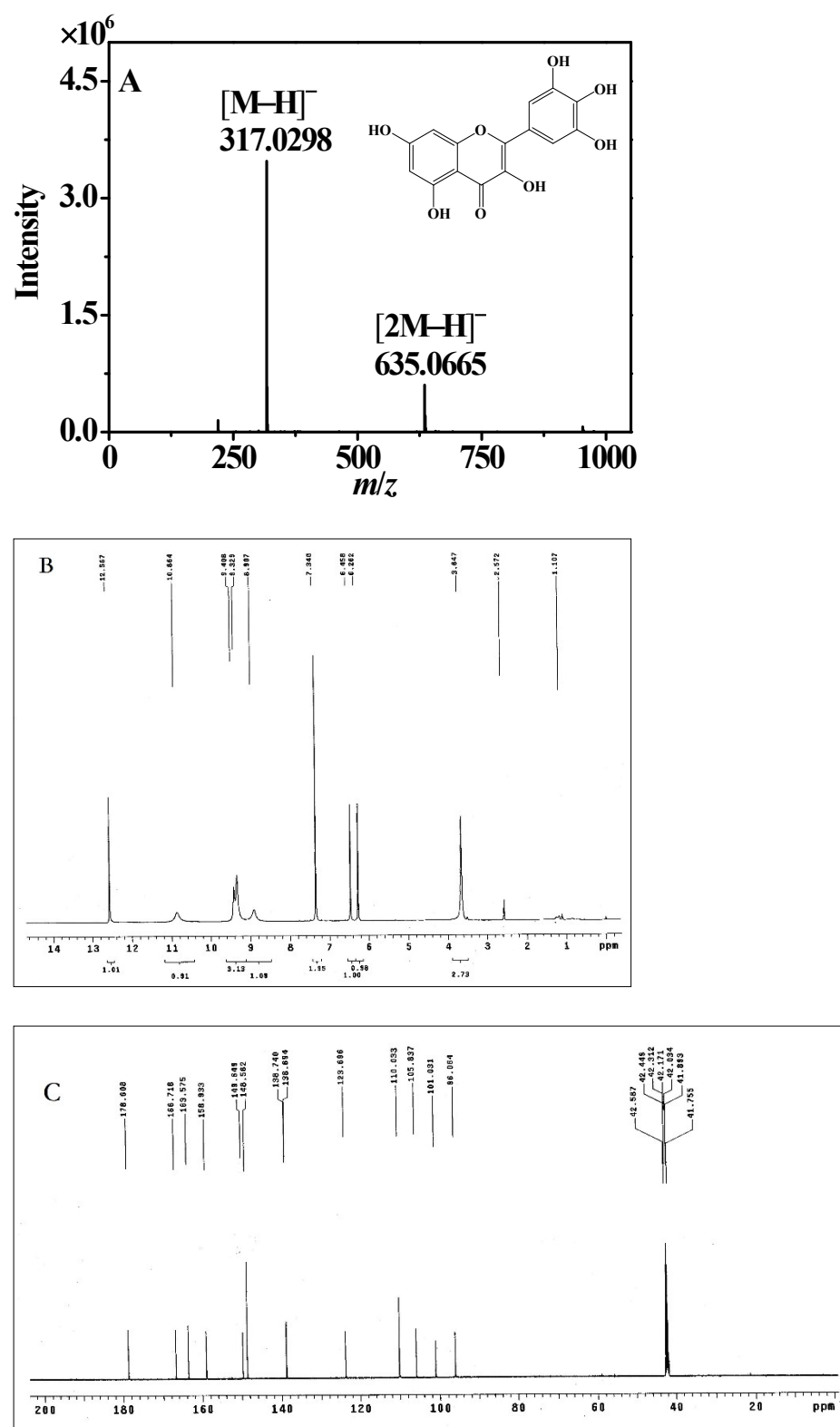


Fig. S1 MS (A), ^1H NMR (B) and ^{13}C NMR (C) spectra of purified myricetin.

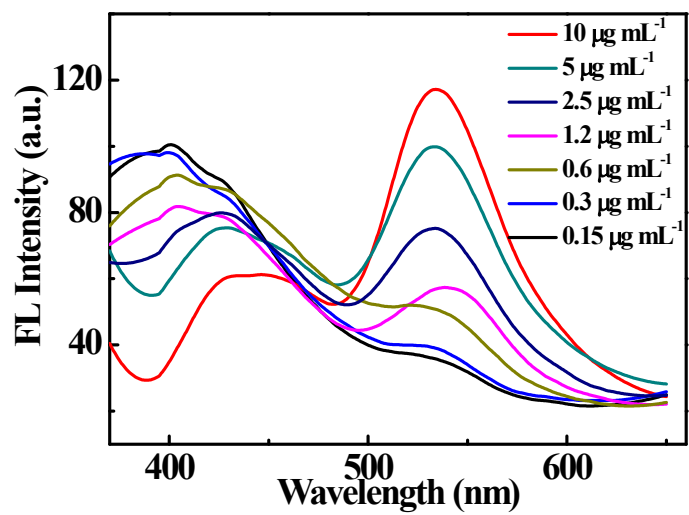


Fig. S2 Concentration dependence of FL spectra of myricetin in THF/H₂O (20/80, v/v) solution.

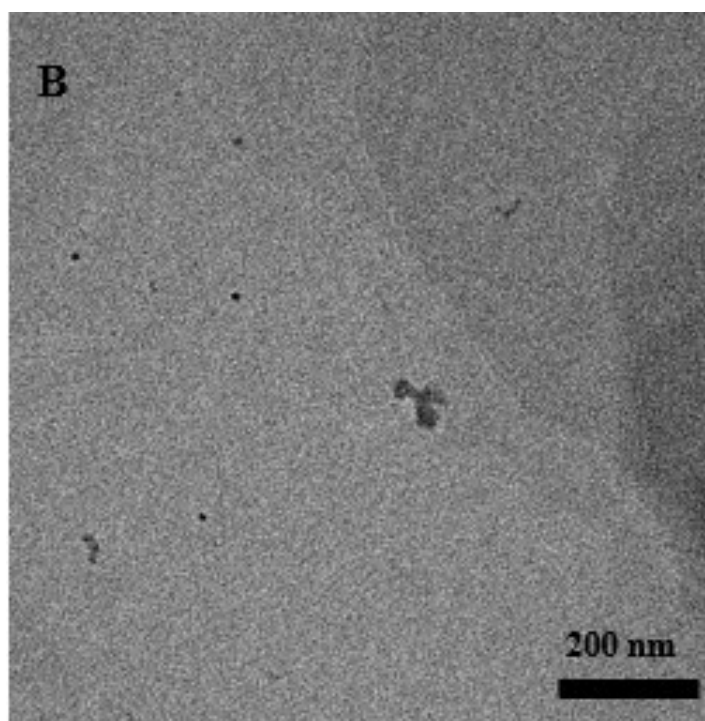
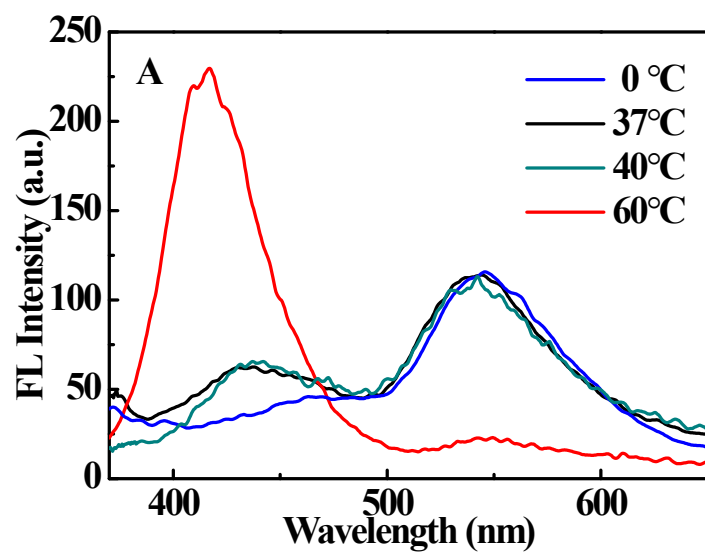


Fig. S3 FL spectra of myricetin crystals at different temperatures (A), TEM image of myricetin crystals at 60 °C (B).

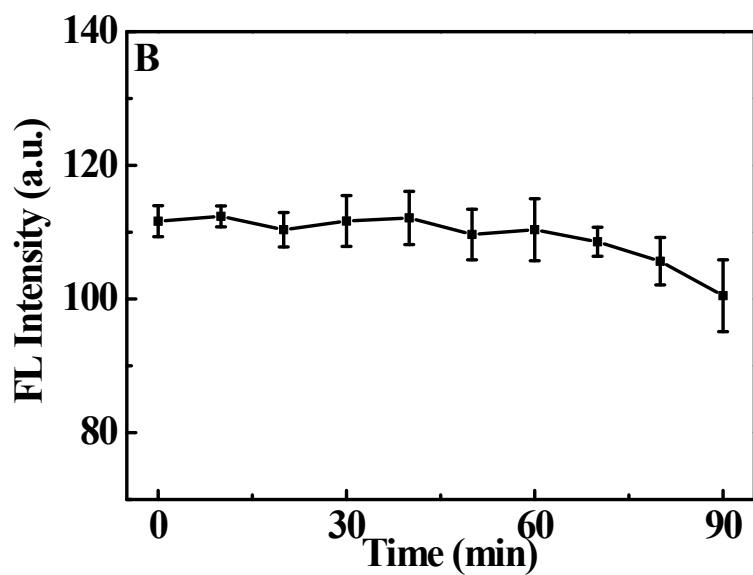
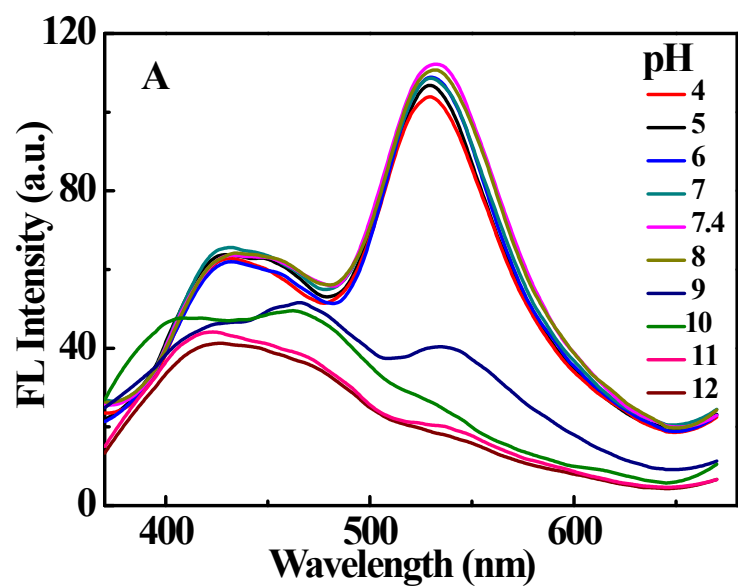


Fig. S4 FL spectra of myricetin crystals under different pH (A); FL intensities of myricetin crystals at 530 nm with different UV irradiation (B).

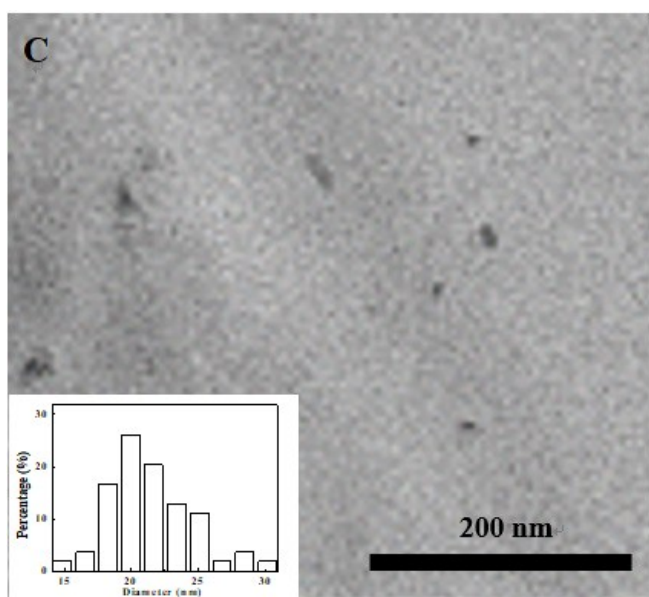
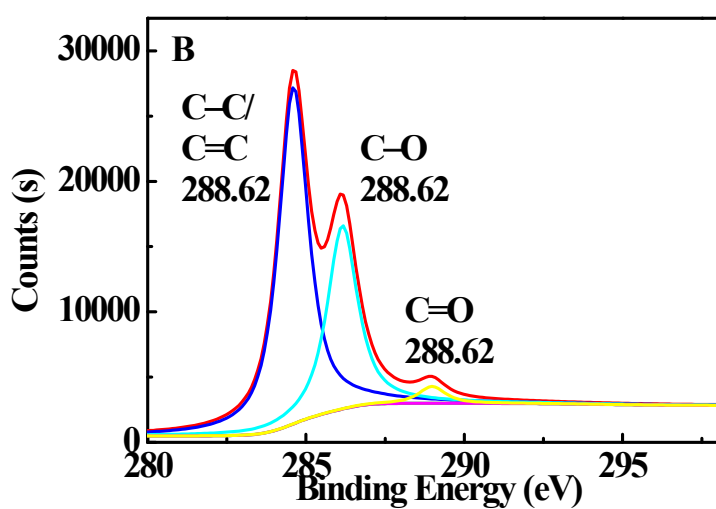
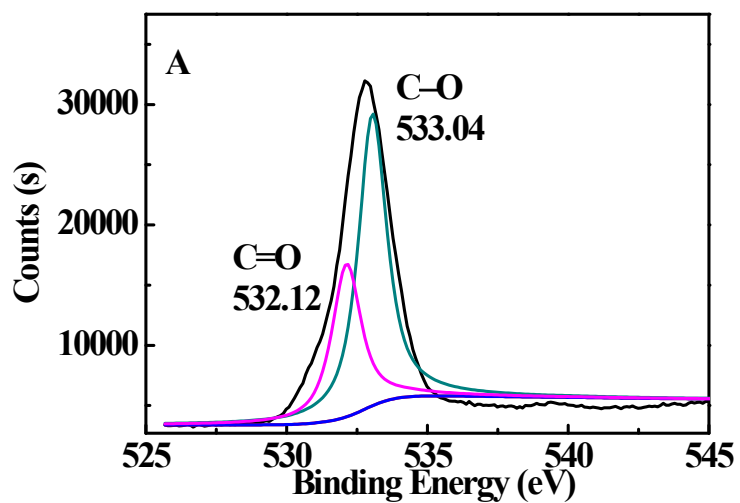


Fig. S5 High resolution XPS spectra of O 1s (A) and C 1s (B) of myricetin nanocrystals; TEM image of myricetin nanocrystals (C).

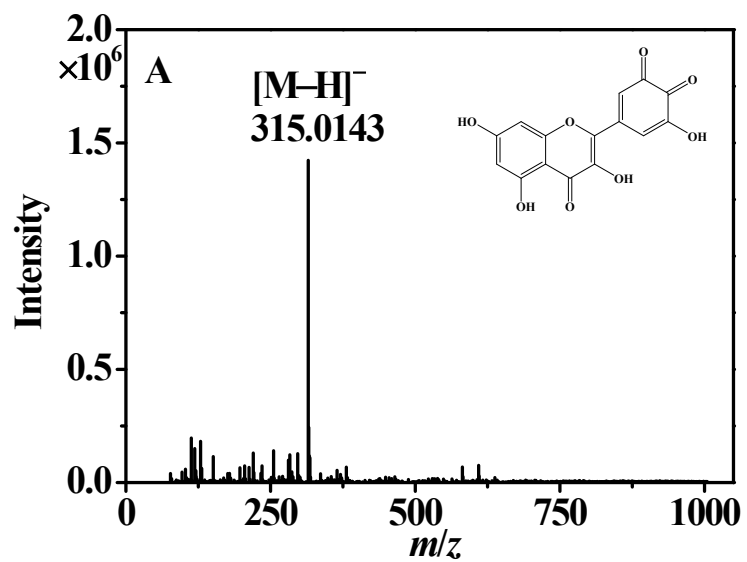


Fig. S6 MS spectrum of myricetin *o*-quinine.

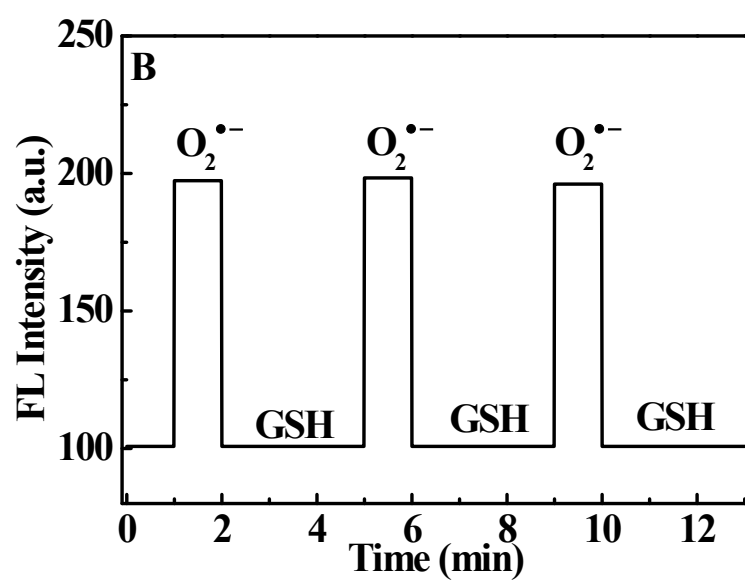
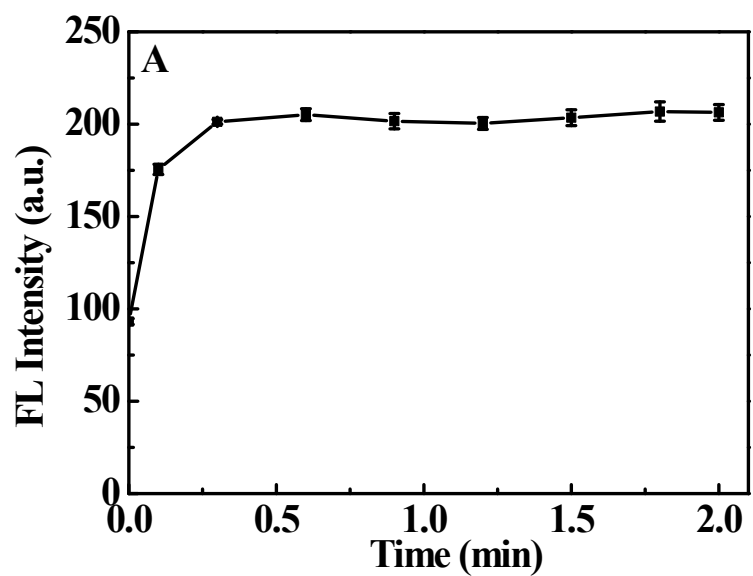


Fig. S7 Effect of time on the myricetin reaction with $O_2^{\bullet-}$ (A); the reversibility of myricetin nanocrystals by addition of $O_2^{\bullet-}$ and glutathione (GSH) in turn (B).

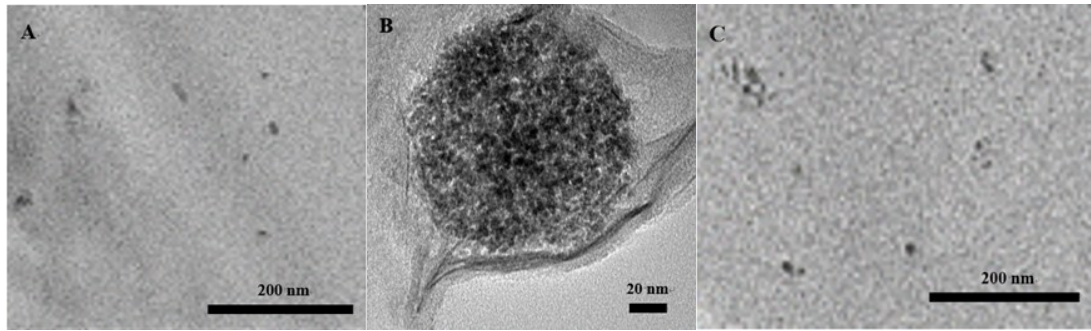


Fig. S8 TEM images of myricetin nanocrystals with different conditions. (A) Myricetin nanocrystals; (B) Myricetin nanocrystals + $O_2^{\cdot-}$; (C) Myricetin nanocrystals + $O_2^{\cdot-}$ + GSH.

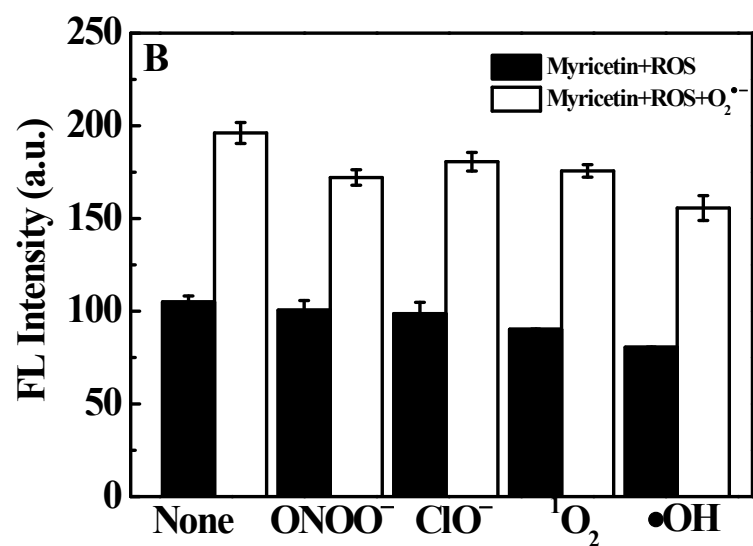
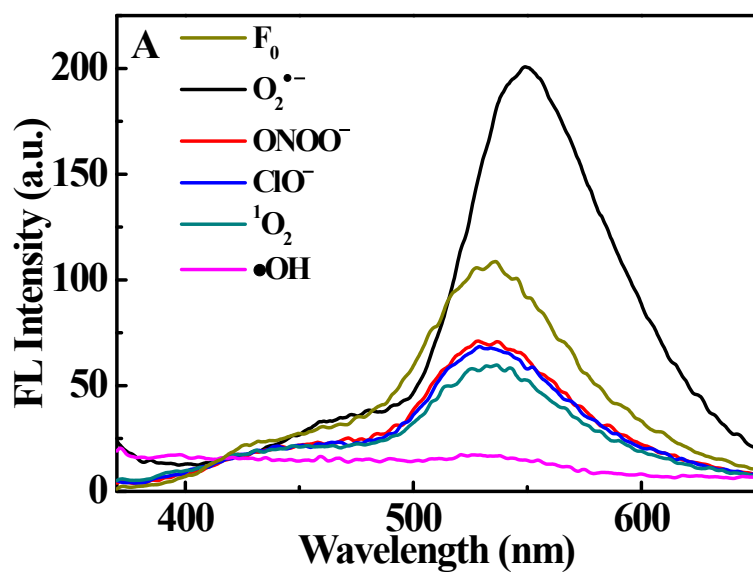


Fig. S9 (A) FL spectra of myricetin nanocrystals after addition of •OH, ¹O₂, ONOO⁻, ClO⁻ and O₂^{•-}, respectively (30 μM); (B) FL intensities of myricetin nanocrystals to various reactive species. Black bars represent the addition of competing ROS (10 μM), and white bars represent the subsequent addition of O₂^{•-} (30 μM) to the solution.

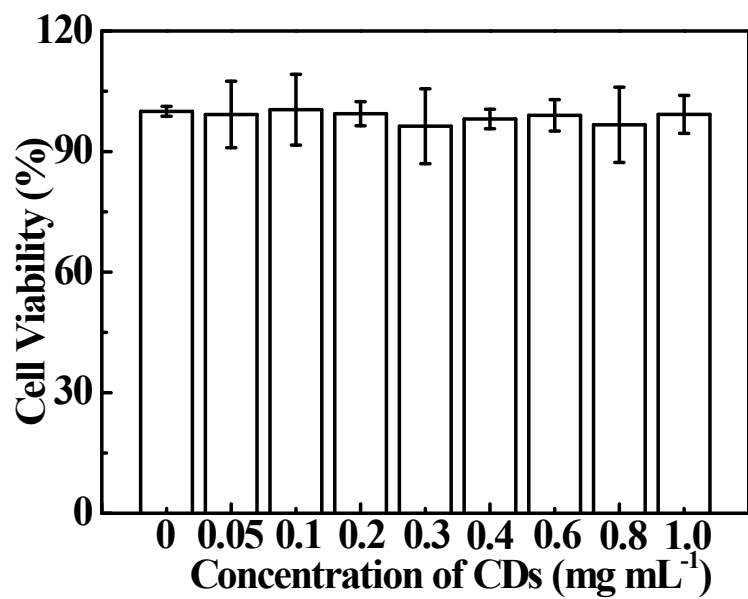


Fig. S9 Cell viabilities of HeLa cells treated with different concentrations of myricetin nanocrystals.